Optics Letters

Flat-gain L-band amplifier containing $AlPO_4$ units in aluminophosphosilicate erbium-doped fibers

Ziwei Zhai,* Arindam Halder, and Jayanta K. Sahu

Optoelectronics Research Centre, University of Southampton, Highfield, Southampton SO17 1BJ, UK
**z.zhai@soton.ac.uk*

Received 21 August 2023; revised 11 September 2023; accepted 2 October 2023; posted 2 October 2023; published 19 October 2023

We present a flat-gain single-stage L-band erbium-doped fiber amplifier (EDFA) with a gain ripple of ±0.7 dB from 1580 to 1615 nm, by using aluminophosphosilicate erbium-doped fiber (APS-EDF) with an estimated $AlPO_4$ composition of 13.3 mol%. A series of APS-EDFs were fabricated with increasing $AlPO_4$ and Er concentrations, while maintaining a low background loss of 0.031 ± 0.005 dB/m and preventing Er ion clustering. The spectroscopic study shows a slightly narrowing Er cross section and flattened emission cross-section spectrum in the L-band with more $AlPO_4$, thus favoring the L-band amplification with an improved gain flatness. Also, the gain coefficient, gain saturation, and temperature-dependent gain characteristics were reported. A better temperature tolerance was observed with increasing $AlPO_4$.

https://doi.org/10.1364/OL.503833

There has been a significant interest in utilizing the aluminophosphosilicate (Al_2O_3–P_2O_5–SiO_2, APS) ternary glass host for developing the rare-earth (RE)-doped fibers due to its unique features over the individual binary Al_2O_3–SiO_2 and P_2O_5–SiO_2 systems. By introducing equimolar amounts of Al_2O_3 and P_2O_5, the $AlPO_4$ unit forms, thanks to the pairing of Al and P, where Al accepts an electron from the P=O bond [1]. The tetrahedral structure of the ≡Al–O–P≡ bond, similar to the ≡Si–O–Si≡ bond, was found to exhibit a similar or even lower refractive index compared to that of the pure silica [1,2]. This property is favorable for the development of large-mode-area (LMA) fibers in high-power applications, requiring a large core size to reduce the power density and a low numerical aperture (NA) to maintain the single-mode operation [3–5]. Improving the solubility of RE ions with suppressed clustering effect is another advantage of the $AlPO_4$ join, where the positive charges of RE ions are shielded by the ≡Al–O–P≡ bonds [3,6,7]. Also, the APS glass composition exhibits remarkable properties in developing photodarkening-resistant ytterbium-doped fibers (YDFs) [5,8] and radiation-hardened erbium-doped fibers (EDFs) and YDFs [6,9].

It has been reported that the spectroscopic characteristics of the APS fibers are dominated by the excess doping of Al_2O_3 or P_2O_5, corresponding to the Al or P that has not bonded into $AlPO_4$ [2,3]. In the C-band, there was one report regarding the Er–Yb-co-doped optical fiber lasers in the P-rich APS host, where the laser slope efficiency decreases with an increase in aluminum content [2]. In the L-band, ytterbium-free erbium-doped all-fiber laser in the Al-rich APS host was reported for an Er_2O_3 concentration of 0.06 mol%, resulting in a slope efficiency of 30% operating at 1584 nm [10]. Also, the C-band amplifier performance was studied on a series of APS-EDFs, showing an improved pump-to-signal power conversion efficiency (PCE) at 1550 nm by forming $AlPO_4$ compared to the PCE of both Al_2O_3–SiO_2-based and P_2O_5–SiO_2-based EDFs [3,11].

However, to our knowledge, there has been no study on the performance of APS-EDFs in the L-band amplifier. It has been shown that phosphosilicate EDFs are more favorable for the L-band amplification compared to aluminosilicate EDFs [12–14]. In this paper, we present a series of P-rich APS fibers with an increasing $AlPO_4$ content, exhibiting an improved L-band amplifier performance compared to the phosphosilicate EDF. An APS-EDF with 13.3 mol% of $AlPO_4$ provided a flat gain with a variation of just ±0.7 dB from 1580 to 1615 nm, without using any additional cost-influencing components like gain-flattening filter (GFF) [15] or building complex amplifier architectures like the Raman-EDFA hybrid amplifier system [16], indicating its potential in the dense wavelength division multiplexed (DWDM) applications. Moreover, the spectroscopic characteristics, pump threshold, gain coefficient, gain saturation, and temperature-dependent amplifier performance have been studied on the APS-EDFs.

In this work, three Er-doped aluminophosphosilicate fibers were designated as APS-EDF1, APS-EDF2, and APS-EDF3, with the basic parameters presented in Table 1. Each fiber was drawn from a preform fabricated in-house using the modified chemical vapor deposition (MCVD) and solution doping process, by engineering the doping concentration to incorporate more Al and form $AlPO_4$. The $AlPO_4$ concentration was estimated to be 6.9 mol% for APS-EDF1, 9.3 mol% for APS-EDF2, and 13.3 mol% for APS-EDF3, based on the refractive index difference (Δn) measured by the fiber refractive index profiler and the core element compositions measured by the electron probe microanalyzer (EPMA). The NA decreased with more $AlPO_4$ incorporation, which was 0.13 for APS-EDF1, 0.11 for

Table 1. Basic Parameters of EDFs in This Work

	APS-EDF1	APS-EDF2	APS-EDF3
$AlPO_4$ (mol%)	6.9	9.3	13.3
NA	0.13	0.11	0.10
Core diameter (μm)	8.4	9.7	10.2
LP11 cutoff (nm)	1200	1150	1130
BL@1200 nm (dB/m)	0.026	0.029	0.036
Abs@980 nm (dB/m)	7.5	7	12
UL@980 nm (%)	3.9	5	5.7
Lifetime (ms)	9.8	10.1	10.2

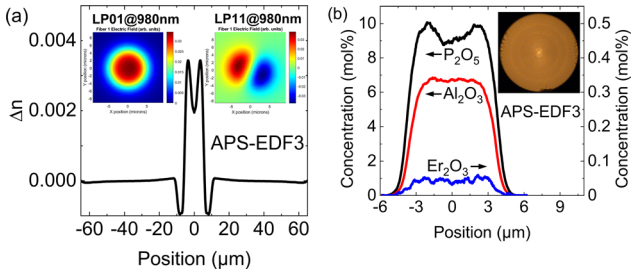

Fig. 1. (a) The refractive index difference (Δn) profile of APS-EDF3. The insets show the 2D profiles of the LP01 and LP11 modes at 980 nm pump wavelength. (b) The core composition distributions (P_2O_5, Al_2O_3, Er_2O_3) of APS-EDF3. The inset shows a microscope image of the fiber end face.

APS-EDF2, and 0.10 for APS-EDF3. The P_2O_5 concentration was maintained to be 8.5–10.5 mol% for the three EDFs. Figures 1(a) and 1(b) show the refractive index difference (Δn) profile and the core composition distributions of APS-EDF3.

With an increasing $AlPO_4$, the background loss (BL) was maintained low, measured to be 0.026 dB/m for APS-EDF1, 0.029 dB/m for APS-EDF2, and 0.036 dB/m for APS-EDF3, using the cutback method. The Er absorption at the 980 nm pump wavelength was measured to be 7.5 dB/m for APS-EDF1, 7 dB/m for APS-EDF2, and 12 dB/m for APS-EDF3. Due to more $AlPO_4$ in the core (13.3 mol%), APS-EDF3 was designed to incorporate more Er ions without clustering [3]. Unsaturable loss (UL) at 980 nm was well controlled, measured to be 3.9% for APS-EDF1, 5% for APS-EDF2, and 5.7% for APS-EDF3 [17]. In addition, one homemade phosphosilicate EDF (P-EDF) with no $AlPO_4$ was selected as a benchmark for comparison purposes, which was designed for the L-band amplifier fabricated using the MCVD and solution doping technique. P-EDF has an NA of 0.23, LP11 cutoff of 1120 nm, Er absorption at 980 nm of 10 dB/m, background loss of 0.05 dB/m, and unsaturable loss at 980 nm of 8.8%.

First, we characterized the spectroscopic properties of the EDFs, by calculating the absorption, emission, and excited-state-absorption cross sections (σ_a, σ_e, and σ_{esa}) from the measured fluorescence intensity, lifetime, and on/off gain [14,18]. Figures 2(a) and 2(b) show the σ_a, σ_e, and σ_{esa} of the three APS-EDFs and the P-EDF. Three P-rich APS-EDFs exhibited similar phosphosilicate host characteristics, with the peak cross section at 1535 nm slightly decreased from 9.7×10^{-25} m^2 (APS-EDF1) to 8.7×10^{-25} m^2 (APS-EDF3). Compared to P-EDF, by forming more $AlPO_4$, a slight narrowing of the peak was observed, together with a slightly reduced ratio of the cross sections at 1480 and 1535 nm [2]. Especially, zooming in on the

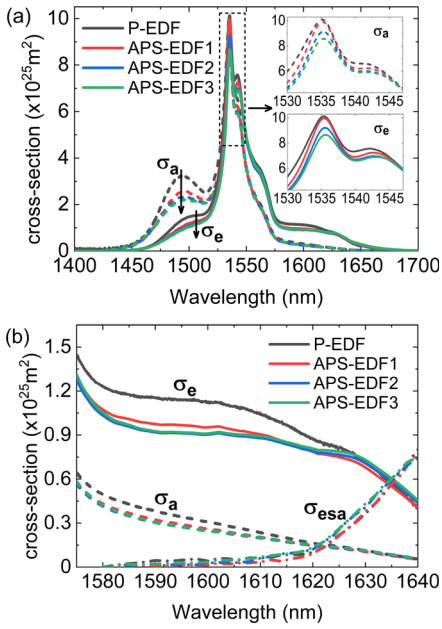

Fig. 2. Cross-section spectra of P-EDF, APS-EDF1, APS-EDF2, and APS-EDF3. (a) σ_a and σ_e spectra from 1400 to 1700 nm. (b) σ_a, σ_e, and σ_{esa} spectra from 1575 to 1640 nm; σ_a, dashed lines; σ_e, solid lines; σ_{esa}, dash-dotted lines. (The arrow direction in (a) indicates the EDF with more $AlPO_4$.)

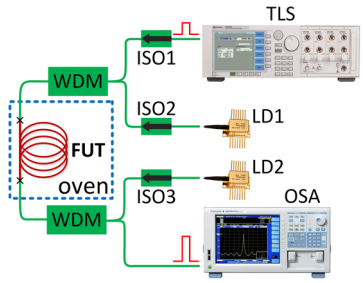

Fig. 3. Schematic of the L-band EDFA experimental setup.

L-band spectrum reveals a flattened σ_e profile, with the potential in improving the L-band gain flatness. And this flattened trend was observed to start saturating when reaching 9.3 mol% of $AlPO_4$, as APS-EDF2. In terms of σ_{esa}, there is no significant difference among all EDFs, with the same cross-point of σ_e and σ_{esa} to be 1634.9 ± 0.1 nm.

Next, the L-band amplifier performance was characterized using the L-band EDFA setup, as illustrated in Fig. 3. A tunable laser source (TLS) provided the input signal from 1580 to 1620 nm with 5 nm steps and −25 dBm power. Yokogawa-AQ6370 optical spectrum analyzer (OSA) was used to capture the input and output signal spectra with a 0.2 nm resolution bandwidth. Wavelength division multiplexers (WDMs) were used to couple the signal and pump. Isolators (ISO) were used to protect the devices. The fiber under test (FUT) was connected in the setup by splicing with the commercial SMF980 (SD362A-00C, Fibercore), which has a core diameter of 4.5 μm, an NA of 0.18, and an LP11 cutoff of 949 nm. The splice loss between the SMF980 and the FUT was taken into consideration for the gain and noise figure (NF) calculation. Two laser diodes (LDs) operating at ~980 nm were used to provide the bi-directional

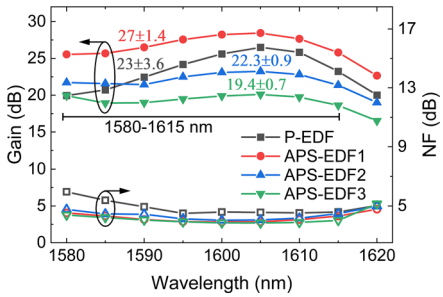

Fig. 4. Gain and NF spectra from 1580 to 1620 nm of P-EDF, APS-EDF1, APS-EDF2, and APS-EDF3 at room temperature (~23°C). The input signal power was –25 dBm.

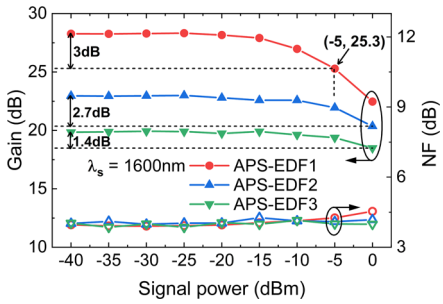

Fig. 5. At 1600 nm, the gain and NF variations with the input signal power increasing from −40 to 0 dBm for APS-EDF1, APS-EDF2, and APS-EDF3 at room temperature (~23°C).

pumps, with a maximum power of ~690 mW measured from the SMF980 after each WDM. The launched pump power was measured after splicing with a small piece of FUT (<4 cm), which was ~564, ~529, ~505, and ~675 mW for APS-EDF1, APS-EDF2, APS-EDF3, and P-EDF, respectively. Using the equal co-propagating and counter-propagating pumps, the total launched pump power was 1128, 1058, 1010, and 1350 mW for APS-EDF1, APS-EDF2, APS-EDF3, and P-EDF, respectively. A thermal oven, operating from −60°C to 80°C, was used to change the environmental temperature of the FUTs for the temperature-dependent amplifier characterizations.

Figure 4 shows the gain and NF spectra at room temperature (~23°C) of APS-EDFs and P-EDF. To achieve a maximum gain at longer wavelengths in the L-band (beyond 1600 nm), the device length was optimized to be 40 m for APS-EDF1 and APS-EDF2, 18 m for APS-EDF3, and 40 m for P-EDF. From 1580–1615 nm, APS-EDFs achieved an improved flat gain of 27 ± 1.4 dB for APS-EDF1, 22.3 ± 0.9 dB for APS-EDF2, and 19.4 ± 0.7 dB for APS-EDF3. The NF was within 4.2 ± 0.3 dB for APS-EDF1, 4.3 ± 0.3 dB for APS-EDF2, and 4.1 ± 0.3 dB for APS-EDF3. However, P-EDF had a higher gain ripple of 23 ± 3.6 dB with a higher NF of 5.2 ± 0.7 dB from 1580 to 1615 nm. The difference in the L-band gain ripple was mainly attributed to the $AlPO_4$ effect on the emission cross-section flatness. At 1620 nm, APS-EDF1 exhibited a 23 dB gain with a 4.7 dB NF, followed by APS-EDF2 with a 19 dB gain and a 5 dB NF, and APS-EDF3 with a 17 dB gain and a 5.1 dB NF. For P-EDF, although providing a similar a 20 dB gain and a 5 dB NF at 1620 nm as APS-EDF2, the higher gain ripple and the higher NF from 1580 to 1615 nm make it less beneficial in the L-band amplifier.

From APS-EDF1 to APS-EDF3, an increasing $AlPO_4$ flattened the gain ripple with a compromised gain value. The fiber core diameters were designed by considering the LP11 mode cutoff wavelength of 1150 ± 50 nm. With a lower NA from more $AlPO_4$, a larger core size was required, resulting in the mode mismatch between the EDF and SMF980 and a higher pump threshold [2]. By simultaneously increasing the co-propagating and counter-propagating pump powers, the pump threshold was measured to be ~400 mW for APS-EDF1, ~475 mW for APS-EDF2, and ~550 mW for APS-EDF3. Also, the overlap between the pump and the fiber core slightly decreased with $AlPO_4$. The overlap factor between the LP01 mode at 980 nm and the doped core region, calculated using the 2D Mode Solver software (Interfiber Analysis LLC), was 0.93, 0.90, and 0.89 for APS-EDF1, APS-EDF2, and APS-EDF3, respectively. In terms of the LP11 mode at 980 nm, the overlap factor was 0.78, 0.76, and 0.72, respectively. It was expected to achieve a similar gain level as APS-EDF1 by increasing the pump power for APS-EDF2 and APS-EDF3. At 1600 nm, the gain coefficient (defined as the maximum ratio of the gain to the pump power) was measured to be 0.027 dB/mW for APS-EDF1, 0.024 dB/mW for APS-EDF2, and 0.020 dB/mW for APS-EDF3. The gain didn't start to saturate within the available pump power in this work. On the other hand, the highly doped APS-EDF3 would require a shortened device length of 18 m, providing a higher gain per unit length compared to APS-EDF1 and APS-EDF2.

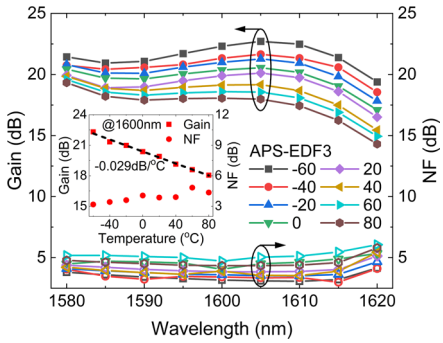

Fig. 6. Gain and NF spectra of APS-EDF3 at different temperatures from −60 to 80°C. The inset shows the gain and NF variations with the temperature at 1600 nm.

Then, the gain saturation of APS-EDFs was studied by measuring the gain and NF variations with the input signal power. Figure 5 shows the gain and NF at 1600 nm of APS-EDFs using an increasing input signal power from −40 to 0 dBm. The saturated output power was 20.3 dBm for APS-EDF1, with a saturated input power of −5 dBm and a corresponding gain of 25.3 dB. A slower gain saturation was observed with more $AlPO_4$. At the input signal power of 0 dBm, the gain drop was 2.7 dB for APS-EDF2 and 1.4 dB for APS-EDF3, compared to the small-signal gain. With a 0 dBm input signal, the pump-to-signal power conversion efficiency (PCE) was found to be 15.5% for APS-EDF1, 10.2% for APS-EDF2, and 6.9% for APS-EDF3.

Furthermore, the gain and NF variations with the environmental temperature were measured, by changing the oven temperature from −60°C to 80°C with 20°C steps. Figure 6 shows the gain and NF spectra at different temperatures of APS-EDF3, with the inset illustrating the gain and NF variations with the temperature at 1600 nm. The temperature-dependent gain (TDG) coefficient, in the unit of dB/°C, was defined as the gain variation with a unit temperature increment. Figure 7 shows the

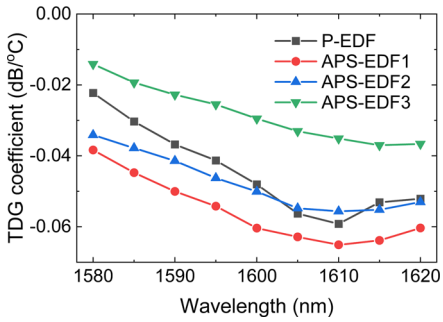

Fig. 7. Temperature-dependent gain (TDG) coefficient spectra of P-EDF, APS-EDF1, APS-EDF2, and APS-EDF3.

TDG coefficient spectra of the three APS-EDFs and P-EDF. At 1600 nm, the TDG coefficient was calculated to be −0.06 dB/°C for APS-EDF1, −0.05 dB/°C for APS-EDF2, −0.029 dB/°C for APS-EDF3, and −0.048 dB/°C for P-EDF. With more $AlPO_4$, the TDG coefficient was smaller (in absolute value), indicating better temperature stability. Such TDG properties were within the phosphosilicate host characteristics [18]. The better temperature tolerance of APS-EDF3 was mainly attributed to a higher $AlPO_4$ and correspondingly reduced amplifier device length.

In conclusion, we fabricated a set of P-rich APS-EDFs with an increasing $AlPO_4$ concentration up to 13.3 mol%, exhibiting a low NA and maintaining a low background loss of 0.031 ± 0.005 dB/m. The absorption, emission, and ESA cross sections were experimentally calculated, still exhibiting a similar characteristics of phosphosilicate EDF, with a cross-point of the emission and ESA cross sections of 1634.9 ± 0.1 nm. With more $AlPO_4$, a slight narrowing of the cross-section peak and the reduced ratio of the cross section at 1480 and 1535 nm were measured. In the L-band spectral region, a flattened emission cross-section profile was observed with more $AlPO_4$, which is expected to achieve a better gain flatness in the amplifier. We have studied the L-band amplifier characteristics of APS-EDFs, achieving a much better gain ripple from 1580 to 1615 nm and a lower NF, compared to the phosphosilicate P-EDF. By increasing $AlPO_4$, the gain flatness has been achieved at ±1.4, ±0.9, and ±0.7 dB for APS-EDF1, APS-EDF2, and APS-EDF3, respectively. A higher pump threshold was observed when increasing $AlPO_4$, with a potential gain improvement by increasing the pump power. Using the available pump in this work, at 1620 nm, we achieved a 23 dB gain with a 4.7 dB NF for APS-EDF1, a 19 dB gain with a 5 dB NF for APS-EDF2, and a 17 dB gain with a 5.1 dB NF for APS-EDF3. Furthermore, the temperature stability on the gain improved with $AlPO_4$. In addition, the APS-EDF3 with the highest $AlPO_4$ content of 13.3%, which has shown superior gain flatness and temperature tolerance, also had a higher Er concentration without Er quenching. Together with a low NA of 0.10, APS-EDF3 is well suited for high-power cladding-pumped fiber lasers. We believe that our results indicate the potential of APS-EDFs in the DWDM L-band amplifiers and for LMA fibers in high-power applications.

Funding. Engineering and Physical Sciences Research Council (EP/W028786/1).

Acknowledgment. The authors are thankful to Dr. Andrew Matzen from the Department of Earth Sciences, University of Oxford, for his valuable support and assistance with the EPMA measurement..

Disclosures. The authors declare no conflicts of interest.

Data availability. The data for this work is accessible through the University of Southampton Institutional Research Repository [19].

REFERENCES

1. D. J. DiGiovanni, J. B. MacChesney, and T. Y. Kometani, J. Non-Cryst. Solids **113**, 58 (1989).
2. G. G. Vienne, W. S. Brocklesby, R. S. Brown, Z. J. Chen, J. D. Minelly, J. E. Roman, and D. N. Payne, Opt. Fiber Technol. **2**, 387 (1996).
3. M. E. Likhachev, M. M. Bubnov, K. V. Zotov, D. S. Lipatov, M. V. Yashkov, and A. N. Guryanov, Opt. Lett. **34**, 3355 (2009).
4. A. Halder, D. Lin, A. A. Umnikov, N. J. Ramírez-Martínez, M. Núñez-Velázquez, P. Barua, S. Alam, and J. K. Sahu, in Conference on Lasers and Electro-Optics (CLEO) (OSA Technical Digest, 2018), paperJTh2A.77.
5. S. Liu, H. Zhan, K. Peng, Y. Li, S. Sun, J. Jiang, L. Ni, X. Wang, J. Yu, L. Jiang, R. Zhu, J. Wang, F. Jing, and A. Lin, Opt. Mater. Express **8**, 2114 (2018).
6. F. Wang, C. Shao, C. Yu, S. Wang, L. Zhang, G. Gao, and L. Hu, J. Appl. Phys. **125**, 173104 (2019).
7. D. S. Lipatov, A. N. Abramov, A. N. Guryanov, K. K. Bobkov, T. S. Zaushitsyna, M. M. Bubnov, and M. E. Likhachev, in Conference on Lasers and Electro-Optics Europe & European Quantum Electronics Conference (CLEO/Europe-EQEC) (OSA Technical Digest, 2021), paper cj_9_2.
8. S. Jetschke, S. Unger, A. Schwuchow, M. Leich, and J. Kirchhof, Opt. Express **16**, 15540 (2008).
9. M. E. Likhachev, M. M. Bubnov, K. V. Zotov, A. L. Tomashuk, D. S. Lipatov, M. V. Yashkov, and A. N. Guryanov, J. Lightwave Technol. **31**, 749 (2013).
10. M. P. Lord, L. Talbot, O. Boily, T. Boilard, G. Gariépy, S. Grelet, P. Paradis, V. Boulanger, N. Grégoire, S. Morency, Y. Messaddeq, and M. Bernier, Opt. Express **28**, 3378 (2020).
11. M. E. Likhachev, K. V. Zotov, M. M. Bubnov, D. S. Lipatov, M. V. Yashkov, and A. N. Guryanov, in European Conference on Optical Communication (ECOC) (2009), paper 10.1.5.
12. M. Kakui and S. Ishikawa, Opt. Commun. **245**, 193 (2005).
13. S. Tanaka, K. Imai, T. Yazaki, H. Tanaka, T. Yamashita, and M. Yoshida, in Optical Fiber Communication Conference (OFC) (OSA Technical Digest, 2002), paper ThJ3.
14. Z. Zhai, A. Halder, M. Nunez-Velazquez, and J. K. Sahu, J. Lightwave Technol. **40**, 4819 (2022).
15. M. Yucel, H. H. Goktas, and F. V. Celebi, Optik **122**, 872 (2011).
16. S. Singh and R. S. Kaler, IEEE Photonics Technol. Lett. **25**, 250 (2013).
17. M. P. Kalita, S. Yoo, and J. K. Sahu, Opt. Express **16**, 21032 (2008).
18. Z. Zhai and J. K. Sahu, J. Lightwave Technol. **41**, 3432 (2023).
19. "Z ZhaiDataset in support of the journal article 'Flat-gain L-band amplifier containing AlPO4 units in alumino-phospho-silicate erbium-doped fibers'," University of Southampton Institutional Research Repository, 2023, https://eprints.soton.ac.uk/482975/.